Biorheology 49 (2012) 301–316
DOI 10.3233/BIR-120620
IOS Press

Charge effects on the hindered transport of macromolecules across the endothelial surface glycocalyx layer

Masako Sugihara-Seki *, Takeshi Akinaga and Hideyuki O-Tani
Department of Pure and Applied Physics, Kansai University, Suita, Osaka, Japan

Abstract. A fluid mechanical and electrostatic model for the transport of solute molecules across the vascular endothelial surface glycocalyx layer (EGL) was developed to study the charge effect on the diffusive and convective transport of the solutes. The solute was assumed to be a spherical particle with a constant surface charge density, and the EGL was represented as an array of periodically arranged circular cylinders of like charge, with a constant surface charge density. By combining the fluid mechanical analyses for the flow around a solute suspended in an electrolyte solution and the electrostatic analyses for the free energy of the interaction between the solute and cylinders based on a mean field theory, we estimated the transport coefficients of the solute across the EGL. Both of diffusive and convective transports are reduced compared to those for an uncharged system, due to the stronger exclusion of the solute that results from the repulsive electrostatic interaction. The model prediction for the reflection coefficient for serum albumin agreed well with experimental observations if the charge density in the EGL is ranged from approximately -10 to -30 mEq/l.

Keywords: Debye–Hückel equation, Boltzmann factor, reflection coefficient, hindrance factors

1. Introduction

It is known that the luminal surface of vascular endothelial cells is covered with a glycocalyx layer, a network of membrane-bound proteoglycans and glycoproteins. The important role of the endothelial surface glycocalyx layer (EGL) has recently been recognized in a variety of processes in cardiovascular physiology and pathophysiology, including microvessel permeability, endothelial mechanotransduction, inflammatory responses, atherosclerosis and diabetes [10,26,29,30,35,37]. Among these, this study is concerned with transport property of the EGL as a molecular filter of plasma proteins. Because of its distinct location in the transvascular pathway, the EGL is considered to form the primary size selective structure to solute molecules in microvessel permeability [9,24,36]. In the present study, we develop a fluid mechanical and electrostatic model for the transport of solute molecules across the EGL. In particular, we focus on the effect of electric charge on the solute transport.

By structural analysis of the EGL in capillaries of frog mesentery, Squire et al. [31] showed that there is an underlying three-dimensional fibrous meshwork within the EGL with characteristic spacings of about 20 nm and proposed a structural model of the EGL, consisting of clusters of fibrous strands projecting normally to the surface of the luminal wall in a regular fashion. It was concluded that this

*Address for correspondence: Prof. Masako Sugihara-Seki, Department of Pure and Applied Physics, Kansai University, 3-3-35 Yamate-cho, Suita, Osaka 564-8680, Japan. Tel./Fax: +81 6 6368 0866; E-mail: sekim@kansai-u.ac.jp.

spacing and a fiber diameter of 10–12 nm provide just the size regime to account for the observed molecular filtering. Recently, Arkill et al. [5] showed evidence of similar structural regularity in the EGL of various mammalian microvessels and it has been suggested that the filtering mechanism of the EGL could be universal in a variety of microvessels.

To characterize transport property of porous membranes, the following equations, called Kedem–Katchalsky equations are often employed [8,19,20].

$$\begin{aligned} J_{\mathrm{s}} &= \omega RT\Delta c_{\infty} + (1-\sigma_{\mathrm{f}})c^{*}J_{\mathrm{v}}, \\ J_{\mathrm{v}} &= L_p(\Delta p_{\infty} - \sigma_{\mathrm{v}}RT\Delta c_{\infty}), \end{aligned} \tag{1}$$

where J_{s} and J_{v} are the solute and solvent fluxes per unit area of membrane, R is the gas constant and T is the absolute temperature. ∞ denotes the bulk solution conditions, and Δc_{∞} and Δp_{∞} are the concentration difference of solutes and the pressure difference across the membrane, respectively. c^{*} represents the solute concentration at the upstream side of the membrane. In these equations, L_p, the hydraulic conductivity, describes the permeability to water and ω, the diffusive permeability, describes the permeability to solutes. σ_{f} is the solvent drag or filtration reflection coefficient that describes the retardation of solutes and σ_{v}, the osmotic reflection coefficient, describes the selectivity to solutes. If Onsager's reciprocity postulate is assumed, it can be shown that σ_{f} and σ_{v} are equal [22].

As a mathematical model for the EGL, Weinbaum et al. [38] proposed a hexagonal arrangement of core proteins with a spacing of 20 nm and a fiber diameter of 12 nm, and estimated the reflection coefficient for serum albumin, which is the most abundant plasma proteins, to be 0.67 using fiber matrix theory [9]. Compared to previous predictions, this estimate provided a better agreement with experimental observations. In a previous study [32], we adopted an idea for membrane transport to develop a fluid mechanical model for transport of solute molecules across the EGL, based on the structural model for the EGL proposed by Squire et al. [31] and Weinbaum et al. [38]. In the EGL model, core proteins were assumed to have a circular cylindrical shape with diameter of 12 nm and to be aligned in parallel to form a hexagonal arrangement with spacing of 20 nm (see Fig. 1). The drag force and the torque exerted on a spherical solute suspended in a fluid between these periodically aligned cylinders were computed, and the obtained values were used to estimate the diffusive permeability ω and the filtration reflection coefficient σ_{f} in Eq. (1) from thermodynamic and mechanical equilibrium relations. The variations of ω and σ_{f} with solute size obtained were found to generally be close to the experimentally measured values. However, the predicted values of the reflection coefficient σ_{f} for some solutes were smaller than the experimentally obtained values. In particular, the reflection coefficients for serum albumin measured in various tissues are typically $>$0.9 [25], whereas the model prediction was as small as approximately 0.74. Although this model prediction explains *in vivo* measurements much better than previous analyses, further study is necessary to account for experimentally observed molecular filtering properties of microvessels.

Although both EGL and serum albumin are negatively charged, our previous study [32] did not consider the charge effect. Due to the repulsive interaction between the EGL and the solute, the solute is more likely to be excluded from the EGL. This in turn could significantly reduce diffusive and convective transport of solutes across the EGL. In the present study, we extend the EGL model in Sugihara-Seki [32] to include the electrostatic effect in such a way that the cylinders and solute have a uniform surface charge and the solvent is an electrolyte solution containing small cations and anions. Similar models for the EGL were adopted to study osmotic flow across the EGL and to estimate the osmotic reflection coefficient σ_{v} in Eq. (1) for the neutral case [40] and for the charged case [6,33]. In Sugihara-Seki

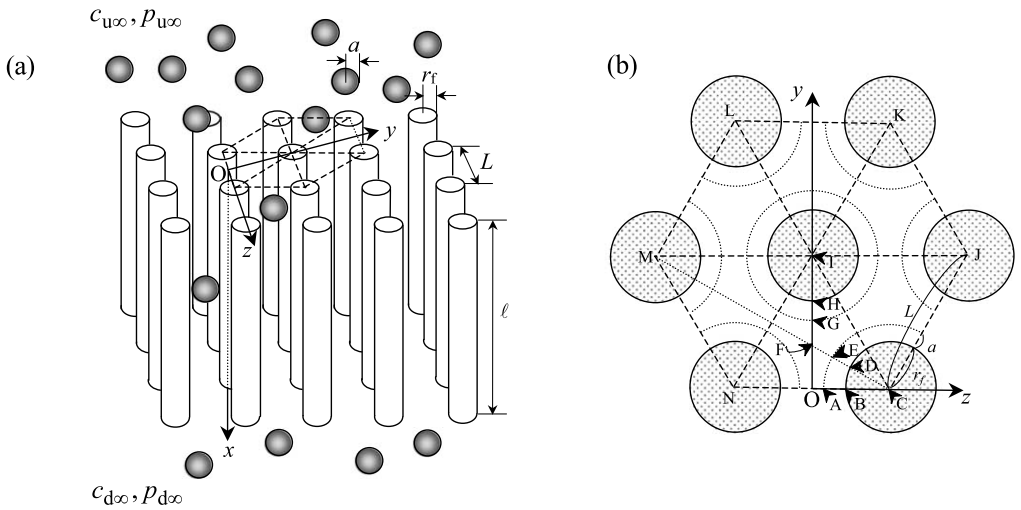

Fig. 1. (a) Sketch of the EGL model consisting of hexagonally arranged circular cylinders of radius r_f. The distance between the centers of adjacent cylinders is L, and the length of the cylinders is l. Spherical solutes of radius a are suspended in an electrolyte solution, which contains small cations and anions. The surfaces of the solutes and the cylinders are electrically charged with densities q_s and q_c, respectively. The EGL model separates bulk solutions with solute concentrations of $c_{u\infty}$ and $c_{d\infty}$ and hydrostatic pressures of $p_{u\infty}$ and $p_{d\infty}$. (b) Cross section of the EGL perpendicular to the cylinder axis. Triangular region OCF is a periodic unit of the cross section. Region OBDF, denoted A', is available for the fluid, and region OAEF, denoted A^*, is available for the center of the solute.

et al. [33], the ions in the electrolyte solution were assumed to be sufficiently small, so that a continuum, point-charge description of the electrostatic double-layers was used. The electrostatic potential in the electrolyte solution around a solute was determined using a linearized form of the Poisson–Boltzmann equation, i.e., the Debye–Hückel equation, to evaluate the interaction energy between the solute and the cylinders. In the present study, the results of the electrostatic interaction energy obtained in Sugihara-Seki et al. [33] are used to estimate the diffusive and convective transport of spherical solutes across the EGL, i.e. ω and σ_f in Eq. (1) in the presence of electric charge.

The objective of the present study is to investigate the electrostatic effect on the transport of spherical solutes across the EGL. Combining a fluid mechanical analysis of the drag forces exerted on a spherical solute and an electrostatic analysis of the interaction energy, we estimate the solute transport coefficients ω and σ_f as a function of the charge densities, the ion concentration, and the solute size.

2. Formulation

We consider the transport of spherical solutes across an EGL model, including the electrostatic interaction between the solute and EGL. The EGL model consists of circular cylinders of radius r_f that are aligned parallel to each other to form a hexagonal arrangement with a spacing L between the centers of neighboring cylinders, as shown in Fig. 1. The width of the layer or the axial length of the cylinders, l, is assumed to be sufficiently large compared to L, so that end effects on the fluid motion and the electric field can be neglected. The layer separates two solutions having different solute concentrations $c_{u\infty}$ and $c_{d\infty}$. The solutes are identical rigid spheres of radius a. The surfaces of the cylinders and the solutes are assumed to have uniformly distributed electric charge with densities of q_c and q_s, respectively. The solutes are suspended in an electrolyte solution containing small cations and anions. The sizes of the

ions are assumed to be small compared to r_{f} and a, so that the ions are regarded as point charges and the electrolyte solution is regarded as a uniform incompressible Newtonian fluid with viscosity μ. We also assume that there is no difference in ion concentrations on either side of the EGL.

We take the x-axis parallel to the axis of the cylinders and the y- and z-axes perpendicular to the x-axis as shown in Fig. 1. A unit of the hexagonal geometry in the cross section is shown in Fig. 1(b). Since the hexagonal region CJKLMN is divided into equal triangular regions such as OCF shown in Fig. 1(b), we confine ourselves to the case where a solute is placed in this triangular region. We denote the area of the triangle OCF as A, that of region OBDF as A', which represents the area available for the fluid, and that of region OAEF as A^*, which is the area available for the center of the solute. Note that line FC is equivalent to line FI.

We are concerned with steady and isothermal transport of the solutes at T(K) along the x-direction. Mechanical and thermal equilibrium in the x-direction requires the hydrodynamic force exerted on a solute to be balanced by the gradient of the chemical potential of the solute. For a solute translating with velocity U in the x-direction, and immersed in a flow of the suspending fluid with mean velocity V, this condition yields

$$kT\frac{1}{c}\frac{\partial c}{\partial x} = 6\pi\mu a(-UF_t + VF_0), \tag{2}$$

where k is the Boltzmann constant and $c(x, y, z)$ is the solute concentration. Coefficients F_t and F_0 represent the drag coefficients defined as $F_t = -F/6\pi\mu aU$ and $F_0 = F'/6\pi\mu aV$, respectively, where F is the hydrodynamic force acting on the solute translating in the x-direction with velocity U in an otherwise quiescent fluid, and F' is the force exerted on a stationary solute immersed in a pressure-driven flow in the x-direction with mean velocity V. Equation (2) corresponds to Eq. (2a) in Sugihara-Seki [32], which indicated that the contributions to solute transport from the chemical potential gradient due to the pressure gradients and the force due to solute rotation are small. These contributions are neglected in Eq. (2).

We further assume thermodynamic equilibrium of solutes in the cross section, so that a Boltzmann distribution of solutes is realized:

$$c(x, y, z) = c_0(x)\exp\left[-\frac{\phi(y, z) - \phi_0}{kT}\right], \tag{3}$$

where $\phi(y, z)$ denotes the solute potential and the subscript 0 indicates values at reference point F (see Fig. 1(b)). Note that point F is equidistant from three adjacent cylinders. The solute potential $\phi(y, z)$ represents the interaction energy between the solute and the cylinders, which depends on the position of the solute center in the cross section. The solute potential for the purely steric condition is given by

$$\phi = \begin{cases} 0 & \text{in region } A^*, \\ \infty & \text{in the remaining region of } A. \end{cases} \tag{4}$$

Thus, in Sugihara-Seki [32], which considered only the steric condition, the solute concentration c was assumed to be a function of only x, corresponding to $c(x, y, z) = c(x)$ in region A^*, as easily deduced from Eqs (3) and (4). In the case considered herein, the solute potential ϕ includes the electrostatic interaction energy as well as the steric restriction between the solute and the cylinders.

From Eq. (2), we obtain an expression for the axial component of the solute flux [17]:

$$\langle N\rangle = -K_{\mathrm{d}} D_\infty \frac{\mathrm{d}\langle c\rangle}{\mathrm{d}x} + K_{\mathrm{c}} V \langle c\rangle, \tag{5}$$

where $N(= cU)$ is the solute flux, the angle brackets indicate the average over A', $D_\infty = kT/(6\pi\mu a)$ represents the diffusivity in an unbounded solution, and K_{d} and K_{c} are the local hindrance factors for diffusion and convection, respectively, and are given as follows:

$$K_{\mathrm{d}} = \frac{\int_{A^*} 1/F_t(y,z)\mathrm{e}^{-\phi(y,z)/kT}\,\mathrm{d}A}{\int_{A^*} \mathrm{e}^{-\phi(y,z)/kT}\,\mathrm{d}A}, \tag{6}$$

$$K_{\mathrm{c}} = \frac{\int_{A^*} F_0(y,z)/F_t(y,z)\mathrm{e}^{-\phi(y,z)/kT}\,\mathrm{d}A}{\int_{A^*} \mathrm{e}^{-\phi(y,z)/kT}\,\mathrm{d}A}, \tag{7}$$

where integrations are performed over A^*. The solution of Eq. (5) can be expressed as:

$$\langle N\rangle = K_{\mathrm{c}} V \frac{\langle c\rangle_{\mathrm{u}} - \langle c\rangle_{\mathrm{d}}\mathrm{e}^{-Pe}}{1-\mathrm{e}^{-Pe}}, \tag{8}$$

where the Peclet number is defined in terms of the length of the cylinders or the thickness, l, of the EGL:

$$Pe = \frac{K_{\mathrm{c}} V l}{K_{\mathrm{d}} D_\infty}. \tag{9}$$

Here, $\langle c\rangle_{\mathrm{u}}$ and $\langle c\rangle_{\mathrm{d}}$ are the averaged solute concentration at the entrance and exit, respectively, of the layer. These quantities are related to the bulk concentrations by

$$\langle c\rangle_{\mathrm{u}} = c_{\mathrm{u}\infty}\Phi, \qquad \langle c\rangle_{\mathrm{d}} = c_{\mathrm{d}\infty}\Phi, \tag{10a,b}$$

$$\Phi = \frac{1}{A'}\int_{A^*} \mathrm{e}^{-\phi(y,z)/kT}\,\mathrm{d}A. \tag{11}$$

The quantity Φ defined by Eq. (11) is referred to as the solute partition coefficient, which represents the cross-sectional average concentration of the solute at either end of the EGL divided by the adjacent external concentration. Substitution of Eqs (10a) and (10b) into Eq. (8) yields:

$$\langle N\rangle = \Phi K_{\mathrm{c}} V c_{\mathrm{u}\infty} \frac{1-(c_{\mathrm{d}\infty}/c_{\mathrm{u}\infty})\mathrm{e}^{-Pe}}{1-\mathrm{e}^{-Pe}}. \tag{12}$$

If we define

$$H = K_{\mathrm{d}}\Phi = \frac{1}{A'}\int_{A^*} \frac{1}{F_t(y,z)}\mathrm{e}^{-\phi(y,z)/kT}\,\mathrm{d}A, \tag{13}$$

$$W = K_{\mathrm{c}}\Phi = \frac{1}{A'}\int_{A^*} \frac{F_0(y,z)}{F_t(y,z)}\mathrm{e}^{-\phi(y,z)/kT}\,\mathrm{d}A, \tag{14}$$

then Eqs (9) and (12) are rewritten as

$$Pe = \frac{WVl}{HD_\infty}, \tag{15}$$

$$\langle N \rangle = WVc_{\mathrm{u}\infty}\frac{1-(c_{\mathrm{d}\infty}/c_{\mathrm{u}\infty})\mathrm{e}^{-Pe}}{1-\mathrm{e}^{-Pe}}. \tag{16}$$

The limiting forms of Eq. (16) are

$$\langle N \rangle = \frac{HD_\infty}{l}(c_{\mathrm{u}\infty} - c_{\mathrm{d}\infty}) \quad \text{for } Pe \ll 1, \tag{17}$$

$$\langle N \rangle = WVc_{\mathrm{u}\infty} \quad \text{for } Pe \gg 1. \tag{18}$$

Note that Eqs (17) and (18) represent diffusive and convective transport, respectively, and H and W are unity for an infinitesimally small solute or in the bulk phase. Thus, the values of H and W represent the hindrance rates for diffusive and convective transport of the solute relative to the corresponding values in the bulk phase, respectively, and are referred to as hindrance factors [17].

The formulation for solute transport presented in Sugihara-Seki [32] was for the purely steric case and is valid for small *Pe*. Since J_s in Eq. (1) and $\langle N \rangle$ are the solute fluxes per area A and A', respectively, the transport coefficients considered, namely, the permeability coefficient ω and the filtration reflection coefficient σ_f in Eq. (1) are related to the hindrance factors H and W in such a way that

$$\omega = \alpha\frac{HD_\infty}{RTl}, \qquad \sigma_\mathrm{f} = 1 - W, \tag{19a,b}$$

where α ($= A'/A$) is the fraction of the surface of the layer occupied by the fluid. In terms of the permeability coefficient for an uncharged solute in the bulk phase, $\omega_\infty (= D_\infty/RTl)$, Eq. (19a) is reduced to

$$\omega/\omega_\infty = \alpha H. \tag{20}$$

In the present study, we calculate Φ, K_d, K_c, H and W as functions of the solute radius, the charge densities, and the ion concentration. In evaluating these values from Eqs (6), (7), (11), (13) and (14), we need (i) to estimate the drag coefficients F_t and F_0 and (ii) to estimate the interaction energy ϕ. We consider the case of a single solute present in each hexagonal region (CJKLMN in Fig. 1(b)), and compute the values of F_t, F_0 and ϕ for this configuration, by using appropriate periodic and symmetric boundary conditions. The procedures (i) and (ii) are described in detail elsewhere [32,33]. In procedure (i), the Stokes equation and the continuity equation were solved using a finite element method for a spherical solute, in the two cases of either the solute translating in the x-direction in an otherwise quiescent fluid or the stationary solute immersed in a pressure-driven flow in the x-direction. The obtained flow fields were used to estimate F_t and F_0 as functions of the position of the solute in the cross section. In procedure (ii), the electrostatic potential in the electrolyte solution around the solute was computed using the Debye–Hückel equation, and the interaction potential energy was obtained as the difference between the free energy of the solute-cylinders system and that of the individual solute and cylinders at infinite separation. In the present analysis, the results reported in Sugihara-Seki et al. [33] were used for $\phi(y, z)$.

The integrations in Eqs (6), (7), (11), (13) and (14) were performed using Gauss–Lobatto–Legendre formulae of the 10th degree. The numerical error was assessed previously [2,3,32].

We confine the present study to the case of univalent anions and cations in the electrolyte, and to solute and cylinders of like charge. For a univalent-univalent electrolyte, the Debye length is defined as $\lambda_D = [\varepsilon RT/2F_a^2 C_\infty]^{1/2}$, where ε is the solvent dielectric permittivity, F_a is the Faraday constant, and C_∞ is the ion concentration in the bulk phase. The Debye length represents the characteristic decay distance of the electrostatic potential from charged surfaces or the thickness of the electrostatic double layer. In terms of the half distance between neighboring cylinders, $L/2$, we define dimensionless lengths $x^* = 2x/L$, $y^* = 2y/L$, and $z^* = 2z/L$ and dimensionless parameters $a^* = 2a/L$ and $\tau = L/2\lambda_D$. The densities of the surface charge on the solute and cylinders q_s and q_c, respectively, are expressed in dimensionless form as $q_\mathrm{s}^* = q_\mathrm{s} L F_a/2\varepsilon RT$ and $q_\mathrm{c}^* = q_\mathrm{c} L F_a/2\varepsilon RT$, respectively.

For the parameter values, we set $L = 20$ nm, $r_\mathrm{f} = 6$ nm [5,31], and $\varepsilon = 6.57 \times 10^{-10}$ C^2/Nm^2, corresponding to aqueous solutions at $T = 310$ K. For $L = 20$ nm, the dimensionless charge density $q_\mathrm{s}^* = q_\mathrm{c}^* = 1$ corresponds to $q_\mathrm{s} = q_\mathrm{c} = 1.75 \times 10^{-3}$ C/m^2. There are no direct measurements of charge densities in the EGL, but several existing estimates are in the range of -1 mEq/l to approximately -35 mEq/l under physiological conditions [1,11,14,18]. The addition of a plasma polyanionic glycoprotein, orosomucoid, to the perfusate was suggested to increase the charge density in the EGL to approximately twice its control value [11,23,39]. If we assume in the present model that all of the electric charge in the EGL is distributed uniformly on the surface of the cylinders, then the charge density, q_c, on the cylinder surface can be expressed in terms of the volumetric charge density, ρ, as $q_\mathrm{c} = \sqrt{3}\rho L^2/(4\pi r_\mathrm{f})$. Adopting this assumption, the charge densities of $\rho = -1, -11.3, -30$ and -60 mEq/l correspond to $q_\mathrm{c} = -0.89 \times 10^{-3}$ C/m^2 ($q_\mathrm{c}^* = -0.51$), -1.00×10^{-2} C/m^2 ($q_\mathrm{c}^* = -5.7$), -2.66×10^{-2} C/m^2 ($q_\mathrm{c}^* = -15.2$), and -5.32×10^{-2} C/m^2 ($q_\mathrm{c}^* = -30.3$), respectively, for $L = 20$ nm and $r_\mathrm{f} = 6$ nm. The charge density on the solute surface, q_s, is also determined by assuming that the net charge of each molecule is distributed uniformly over the surface of the sphere. For example, $q_\mathrm{s} = -1.7 \times 10^{-2}$ C/m^2 ($q_\mathrm{s}^* = -9.5$) for serum albumin with $a = 3.6$ nm and net charge $= -17$ and $q_\mathrm{s} = -3.4 \times 10^{-2}$ C/m^2 ($q_\mathrm{s}^* = -19.6$) for α-lactalbumin with $a = 2.0$ nm and net charge $= -11$. The ion concentrations $C_\infty = 0.01, 0.02, 0.04, 0.1$ and 0.15 M correspond to $\tau = 3.32, 4.69, 6.63, 10.49$ and 12.84, respectively.

3. Results

The drag coefficients F_t and F_0 were computed for solutes of radius $a = 1 - 3.6$ nm ($a^* = 0.1$–0.36) located at various positions in the cross section. The results for $1/F_t$ and F_0/F_t are plotted as functions of the position of the solute center in Fig. 2(a) and (b), respectively, when the solute center is located on the y^*-axis (line OG) or the z^*-axis (line OA). Note that line FG is equivalent to line FE. The values of $1/F_t$ and F_0/F_t, agree well with the corresponding values in Sugihara-Seki [32], which treated the cases of $a^* \geqslant 0.2$. The current computations were performed with a finer mesh at higher accuracy, but the differences between the two results are at most 3%. Both $1/F_t$ and F_0/F_t vanish when the solute center is located on arc AE in Fig. 1(b), i.e., at point G (E) on the y^*-axis or at point A on the z^*-axis. Figure 2(a) indicates that the values of $1/F_t$ are almost constant until the solute center very closely approaches these points. Figure 2(b) shows that the values of F_0/F_t vary gradually along the y^*-axis and reach a maximum at point F, indicated by the vertical thin solid line in Fig. 2(b). The thin dotted line in Fig. 2(b) represents the velocity profile of the suspending fluid driven by a constant pressure gradient

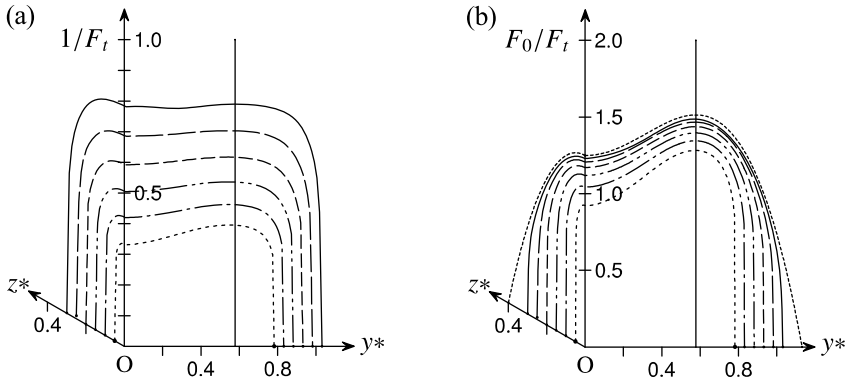

Fig. 2. (a) Plot of $1/F_t$ for $a^* = 0.1$ (solid lines), 0.15 (long dashed lines), 0.20 (dashed lines), 0.25 (dash-double dotted lines), 0.3 (dash-dotted lines) and 0.35 (dotted lines). (b) Plot of F_0/F_t for $a^* = 0.1$ (solid lines), 0.15 (long dashed lines), 0.20 (dashed lines), 0.25 (dash-double dotted lines), 0.3 (dash-dotted lines) and 0.35 (dotted lines). The thin dotted line represents the case of $a^* = 0$, or the velocity profile of the fluid in the absence of the solute relative to the mean fluid velocity. The vertical thin solid line represents the position of point F.

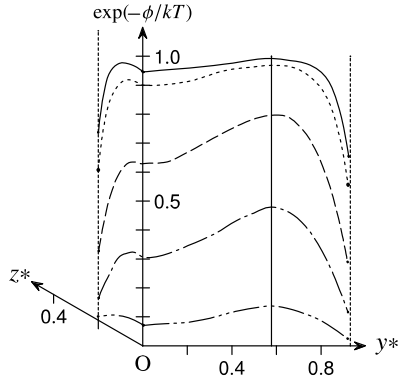

Fig. 3. Boltzmann factor $\exp(-\phi(y^*, z^*)/kT)$ for $a^* = 0.2$, $q_s^* = q_c^* = -5.7$, $\tau = 3.32$ (dash-double dotted lines), 4.69 (dash–dotted lines), 6.63 (dashed lines), 10.49 (dotted lines) and 12.84 (solid lines). The vertical thin solid line represents the position of point F.

in the absence of solutes, which corresponds to the translation velocity of a force-free infinitesimally small solute. Since F_0/F_t is equal to the translation velocity of a freely floating solute relative to the mean fluid velocity, U/V, Fig. 2(b) indicates that the translation velocity of a force-free solute of finite size is always smaller than the local undisturbed fluid velocity evaluated at the center of the solute, but is larger than the mean fluid velocity except very close to the cylinder surface. Note that the rotational motion of the solute has little effect on the drag force compared to the effect of the translating motion, as shown in Sugihara-Seki [32].

As an example of the results for the interaction energy ϕ, Fig. 3 shows the Boltzmann factor $\exp(-\phi/kT)$ for $a^* = 0.2$, $q_s^* = q_c^* = -5.7$, $\tau = 3.32$, 4.69, 6.63, 10.49 and 12.84, when the solute center is located on the y^*-axis or the z^*-axis. Figure 3 clearly indicates a decrease in the Boltzmann factor with decreasing τ or decreasing ion concentration. This trend implies that a decrease in ion concentration enhances the repulsive electrostatic interaction between the solute and the cylinders, which reduces the probability of solute existence in the EGL. For a similar reason, it can be shown that an increase

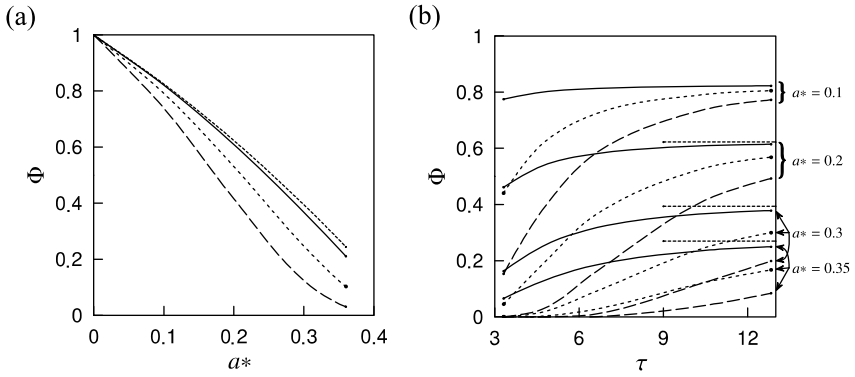

Fig. 4. (a) Partition coefficient Φ as a function of a^* for $q_s^* = -5.7$ and $q_c^* = -0.51$ (solid line), -5.7 (dotted line) and -15.2 (dashed line) at $\tau = 10.49$. The thin dotted line represents Φ in the uncharged case ($q_s^* = q_c^* = 0$). (b) Partition coefficient Φ as a function of τ for $a^* = 0.1$, 0.2, 0.3 and 0.35 at $q_s^* = -5.7$ and $q_c^* = -0.51$ (solid lines), -5.7 (dotted lines) and -15.2 (dashed lines). The thin dotted lines on the right-hand side represent asymptotic values at high ion concentration or the uncharged case.

in charge density $|q_s^*|$ or $|q_c^*|$ increases the interaction energy, resulting in a decrease in the Boltzmann factor. Figure 3 shows that, for constant τ, the Boltzmann factor becomes a maximum at point F along the y^*-axis, indicating that the solute is most likely to be located at point F than at the other sites in the cross section.

As defined in Eq. (11), the integration of the Boltzmann factor over the cross section yields the partition coefficient, which represents the averaged probability of solute existence in the EGL relative to the bulk phase. The obtained values of the partition coefficient Φ are plotted in Fig. 4(a) and (b) as a function of the solute size a^* for $q_s^* = -5.7$ and $\tau = 10.49$ and as a function of τ for $q_s^* = -5.7$, $a^* = 0.1$, 0.2, 0.3 and 0.35. The charge density on the cylinders is chosen as $q_c^* = -0.51, -5.7$ and -15.2. In Fig. 4(a), the thin dotted line represents the uncharged case of $q_s^* = q_c^* = 0$. Figure 4(a) shows that Φ decreases with increasing a^* or $|q_c^*|$. A similar tendency is observed when $|q_s^*|$ is increased. The decrease in Φ is due to an increase in the repulsive electrostatic interaction, which decreases the Boltzmann factor. In Fig. 4(b), the horizontal thin dotted lines on the right-hand side indicate asymptotic values approached at high ion concentration or the uncharged case of $q_s^* = q_c^* = 0$. Figure 4(b) shows a decrease in Φ with decreasing τ. This trend is also explained by an increase in the interaction energy induced by a decrease in τ.

The local hindrance factors K_d and K_c are plotted in Figs 5 and 6, as functions of the solute size a^* for $q_s^* = -5.7$, $\tau = 10.49$ and $q_c^* = -0.51, -5.7$ and -15.2. For reference, K_d and K_c in the uncharged case ($q_s^* = q_c^* = 0$) are also shown by thin dotted lines in Figs 5 and 6, respectively, but the line in Fig. 5 is visually indistinguishable from the solid line for $q_s^* = -5.7$ and $q_c^* = -0.51$. It is interesting to note that K_d is smaller than unity, whereas K_c is larger than unity in the range of a^* examined, irrespective of the existence of an electric charge. This reflects the fact that $1/F_t$ is smaller than unity (see Fig. 2(a)), whereas F_0/F_t is larger than unity on average (see Fig. 2(b)). Equation (5) indicates that local diffusion is smaller and local convection is larger in the EGL compared to the bulk phase.

Figure 5 shows that, for a constant charge density including the no-charge case, K_d declines monotonically as a^* increases. An increase in $|q_c^*|$ increases K_d slightly, but all lines shown in Fig. 5 are close to each other, indicating that the charge density q_c^* has only a slight effect on K_d. Since variations of q_s^* or τ can also be shown not to affect K_d significantly, it is concluded that the electrostatic effect on K_d is small.

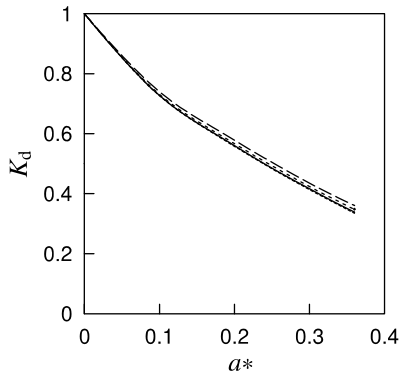

Fig. 5. Local hindrance factor K_d as a function of a^* for $q_s^* = -5.7$ and $q_c^* = -0.51$ (solid line), -5.7 (dotted line) and -15.2 (dashed line) at $\tau = 10.49$. The values of K_d in the uncharged case are plotted by a thin dotted line, which is visually indistinguishable from the solid line.

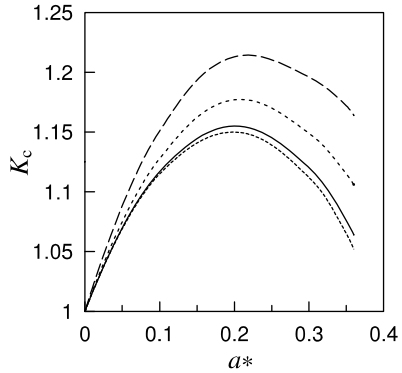

Fig. 6. Local hindrance factor K_c as a function of a^* for $q_s^* = -5.7$ and $q_c^* = -0.51$ (solid line), -5.7 (dotted line) and -15.2 (dashed line) at $\tau = 10.49$. The thin dotted line represents K_c in the uncharged case.

Figure 6 shows that K_c for constant q_c^* increases from unity as the solute size increases from zero, and reaches a maximum value at a certain a^*, followed by a decrease to zero in the limit of the solute touching the three adjacent cylinders at the critical solute radius, $a^* = 2/\sqrt{3} - 2r_f/L \approx 0.555$. The initial increase in K_c with a^* may be counter-intuitive, since a monotonic decrease in K_c with a^* may be expected. From the definition (Eq. (7)), the local hindrance factor K_c represents an average of F_0/F_t or the translation velocity of a force-free solute relative to the mean fluid velocity, U/V, over the area A^*. Thus, the behavior of F_0/F_t (or U/V) shown in Fig. 2(b) may be helpful to understand this trend. As noted above, F_0/F_t (or U/V) decreases to zero as the solute center approaches point G (E) or point A in Fig. 1(b). Figure 2(b) shows that, in the limit of $a^* = 0$, the thin dotted line of F_0/F_t (or U/V) decreases gradually to zero, whereas the rate of decrease increases with solute size. This implies that the translation velocity of larger solutes does not diminish until their centers closely approach point G (E) or point A. In other words, there is a thin layer adjacent to arc AE in Fig. 1(b), where the solute velocity is low, and the layer becomes thinner for larger solute size. This may be responsible for the increase in K_c, i.e., the increase in the average solute velocity, with increasing a^*.

Figure 6 shows that K_c increases as the charge density $|q_c^*|$ is increased. This is because, as the repulsive electrostatic interaction is increased due to either by an increase in the charge density or a decrease in τ, the Boltzmann factor decreases as shown in Fig. 3 and the probability of solute existence near point F (Fig. 1(b)) becomes higher compared to the other sites in the cross section. Consequently, the solute is more likely to be located near point F, which is most away from neighboring cylinder surfaces which impede solute motion. This enhances the translation velocity of the solute, and therefore, increases the convective transport.

While the repulsive electrostatic interaction enlarges the local hindrance factors K_d and K_c, it reduces the hindrance factors H and W, as shown in Figs 7 and 8. An increase in $|q_c^*|$ or a decrease in τ diminishes H and W. A comparison of Fig. 4 and Figs 7 or 8 reveals that the variations of H and W with q_c^*, τ, or a^* are parallel to the corresponding variations of Φ. Thus, the leading determinant of H and W is found to be Φ, and K_d or K_c has only a slight effect (see Eqs (13) and (14)). As the repulsive electrostatic interaction is increased, either by increasing $|q_s^*|$ or $|q_c^*|$ or by decreasing τ, a decrease in Φ makes up for an increase in K_d or K_c to decrease H and W. Note that $W > H$ in the range of a^* examined. This result reflects that K_d is smaller than K_c, as shown in Figs 5 and 6, implying that hindrances are less

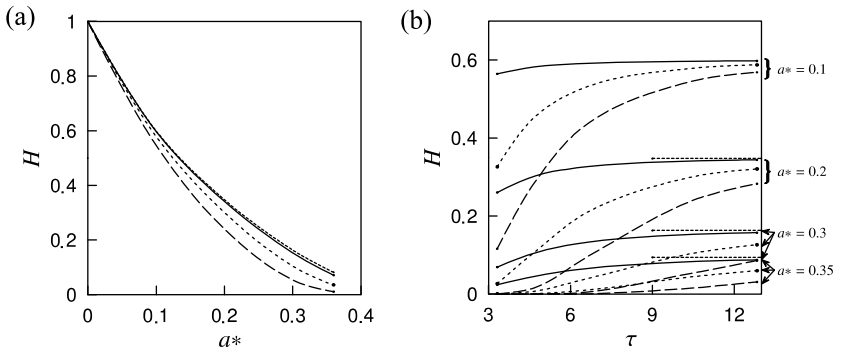

Fig. 7. (a) Hindrance factor H as a function of a^* for $q_s^* = -5.7$ and $q_c^* = -0.51$ (solid line), -5.7 (dotted line) and -15.2 (dashed line) at $\tau = 10.49$. The thin dotted line represents H in the uncharged case. (b) Hindrance factor H as a function of τ for $a^* = 0.1, 0.2, 0.3$ and 0.35 at $q_s^* = -5.7$ and $q_c^* = -0.51$ (solid lines), -5.7 (dotted lines) and -15.2 (dashed lines). The thin dotted lines on the right-hand side represent asymptotic values at high ion concentration or the uncharged case.

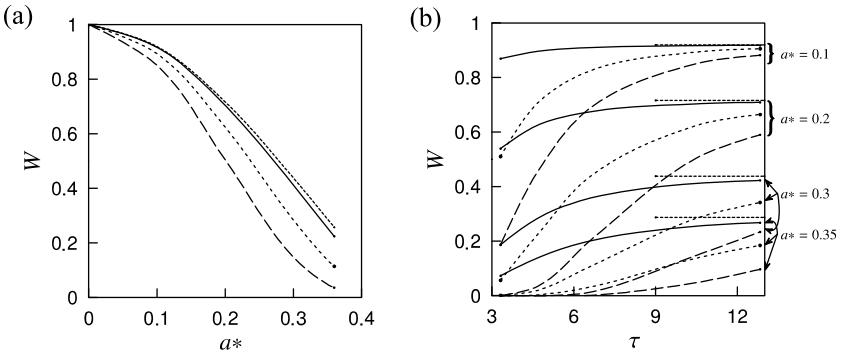

Fig. 8. (a) Hindrance factor W as a function of a^* for $q_s^* = -5.7$ and $q_c^* = -0.51$ (solid line), -5.7 (dotted line) and -15.2 (dashed line) at $\tau = 10.49$. The thin dotted line represents W in the uncharged case. (b) Hindrance factor W as a function of τ for $a^* = 0.1, 0.2, 0.3$ and 0.35 at $q_s^* = -5.7$ and $q_c^* = -0.51$ (solid lines), -5.7 (dotted lines) and -15.2 (dashed lines). The thin dotted lines on the right-hand side represent asymptotic values at high ion concentration or the uncharged case.

pronounced for convection than for diffusion [15,27]. However, the lines shown in Fig. 7(a) are closer to each other than the lines in Fig. 8(a), indicating that the charge effects on the hindrances are larger for convection than for diffusion.

In normal physiological states, the ion concentration is $C_\infty \approx 0.15$ M. From the relationships of Eqs (19b) and (20), the permeability coefficient relative to that for an uncharged solute in the bulk phase, ω/ω_∞, and the filtration reflection coefficient, σ_f, are calculated at $C_\infty \approx 0.15$ M ($\tau = 12.84$), using the obtained values of H and W. The results are plotted in Fig. 9 for $q_s^* = -5.7$ and $q_c^* = -0.51, -5.7$ and -15.2. For comparison, the values of ω/ω_∞ and σ_f in the uncharged case are plotted by thin dotted lines. These thin dotted lines agree well with the corresponding curves in Sugihara-Seki [32]. Figure 9(a) and (b) shows that ω/ω_∞ decreases and σ_f increases monotonically with a^* or $|q_c^*|$. Also plotted in Fig. 9(b) are the experimental values of the reflection coefficient for NaCl, glucose, sucrose, vitamin B_{12}, and albumin in individually perfused capillaries of frog mesentery reported in Curry [8]. The reflection coefficient to serum albumin measured in single rat venules was reported to be 0.94 [21]. Michel and Curry [25] summarized the experimental values of the reflection coefficient for serum albumin measured in various tissues, which are typically greater than 0.9. These values are

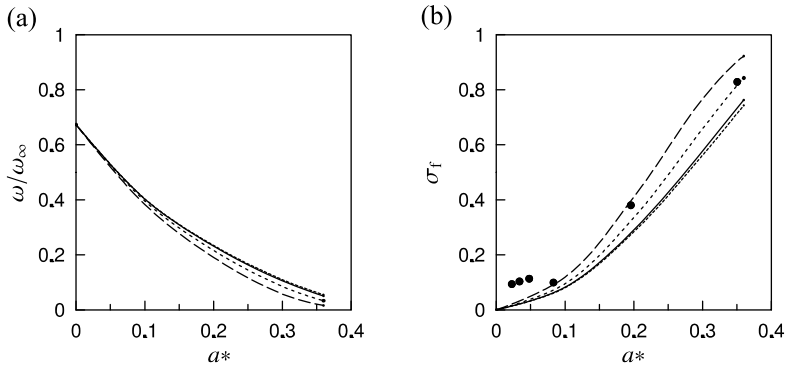

Fig. 9. (a) The diffusive permeability normalized by the unrestricted permeability ω/ω_∞ as a function of a^* for $q_s^* = -5.7$ and $q_c^* = -0.51$ (solid line), -5.7 (dotted line) and -15.2 (dashed line) at $\tau = 12.84$. The values of ω/ω_∞ in the uncharged case are plotted by the thin dotted line, which almost overlaps the solid line. (b) The filtration reflection coefficient σ_f as a function of a^* for $q_s^* = -5.7$ and $q_c^* = -0.51$ (solid line), -5.7 (dotted line) and -15.2 (dashed line) at $\tau = 12.84$. The thin dotted line represents σ_f in the uncharged case. The closed circles represent the experimental results [8].

even larger than the corresponding value reported by Curry [8] (see Fig. 9(b)). Since the charge density of each molecule is not necessarily equal to $q_s^* = -5.7$, we cannot directly compare the experimental results with the curves shown in Fig. 9(b). Nevertheless, the values indicated by the thin dotted line for the uncharged case shown in Fig. 9(b) appear to be far smaller than the experimentally measured values. The present model study predicted that for $a^* = 0.36$ and $q_s^* = -9.5$ corresponding to serum albumin with a net charge $= -17$, the reflection coefficient σ_f is 0.770, 0.784, 0.882, 0.953, and 0.986 at $q_c^* = 0, -0.51, -5.7, -15.2$ and -30.3, respectively, for $C_\infty = 0.15$ M ($\tau = 12.84$). This suggests that $|q_c^*|$ should be in the range from approximately 5.7–15.2 (0.01 C/m^2 $< |q_c| <$ 0.027 C/m^2) in order to account for the experimental results for serum albumin, indicating that $|\rho|$ in the EGL is between approximately 10 and 30 mEq/l.

4. Discussion

A computational model was developed to describe diffusive and convective transport of charged spherical solutes across an EGL model consisting of regular arrays of charged fibers. We have assumed that the fibers are circular cylinders arranged in a hexagonal array and that the flow is parallel to the cylinder axes. Previously, we estimated the permeability coefficient ω and filtration reflection coefficient σ_f of solutes for the uncharged case [32]. A major difference between that study and the present study lies in the solute potential $\phi(y, z)$ that appears in Eqs (11), (13) and (14), where $\phi(y, z)$ represents only steric exclusion in the uncharged case (see Eq. (4)) and includes the electrostatic interaction in the charged case. In the present study, we consider solutes and cylinders of like charge so that the electrostatic interaction between them is repulsive. Accordingly, the Boltzmann factor $\exp(-\phi(y, z)/kT)$ in the charged case is less than unity inside the EGL, and thus the partition coefficient Φ is decreased compared to that in the uncharged case with the other parameters unchanged. Although K_d and K_c are increased due to the repulsive electrostatic interaction, the decrease in the partition coefficient is found to diminish the hindrance factors H and W, and consequently to decrease ω and increase σ_f substantially when the repulsive electrostatic interaction is increased.

In solving the electrostatic potential around a solute placed between circular cylinders, we adopted the Debye–Hückel equation, a linearized form of the so-called Poisson–Boltzmann equation. The difference

of solutions between these two equations has been carefully examined in our previous study [2], for transport of charged spherical solutes through circular cylindrical pores of like charge. In general, the difference becomes larger with decreasing the ion concentration and increasing the charge densities and the solute size. In the case of low charge densities on the solute and pore of -0.005 C/m^2 (dimensionless charge density $= -2.85$), the relative differences of the partition coefficient are within 1% for the solute radius smaller than 3.6 nm ($a^* = 0.36$) and the ion concentration larger than 0.04 M ($\tau = 6.63$). In the case of high charge densities of -0.02 C/m^2 (dimensionless charge density $= -11.4$), on the other hand, the differences are about 10% for $a = 3.6$ nm ($a^* = 0.36$) and $C_\infty = 0.07$ M ($\tau = 8.77$) and they decrease for smaller a^* and larger C_∞ (larger τ). Since the parameter ranges examined in Akinaga et al. [2] are comparable to those in the current study, it could be concluded that the error due to adopting the Debye–Hückel equation instead of the Poisson–Boltzmann equation is small, and its effects on the values of Φ, K_d, K_c, H and W are not significant.

For neutral solutes and cylinders in the same geometry, Zhang et al. [40] analyzed osmotic flow across an EGL by applying the thermodynamic theory for osmotic flow through porous membranes developed by Anderson and Malone [4]. Instead of a rigorous treatment of the hexagonal geometry of the cylinders, they adopted an approximation in which the geometry is replaced by an equivalent fluid annulus around each cylinder and estimated the osmotic reflection coefficient σ_v as a function of the solute radius and the cylinder radius relative to the outer radius of the fluid annulus. Adopting the same approximate treatment of the equivalent fluid annulus together with a pairwise additivity approximation for estimating the electrostatic interaction, Bhalla and Deen [6] examined osmotic flow through an EGL model in the presence of an electric charge on the solute and cylinders. Sugihara-Seki et al. [33] also studied the charge effect on osmotic flow across the EGL model by a numerical analysis without using the equivalent annulus and pairwise additivity approximations. Although the values of the osmotic reflection coefficient σ_v in the uncharged case obtained for various solute size ratios by Zhang et al. [40] turn out to agree remarkably well with the corresponding results obtained by Sugihara-Seki et al. [33], there are some differences in σ_v for the charged case between Sugihara-Seki et al. [33] and Bhalla and Deen [6], probably due to the different electrostatic analysis methods. In the case of $C_\infty = 0.15$ M ($\tau = 12.84$), for example, the osmotic reflection coefficient σ_v for serum albumin is 0.75 in Bhalla and Deen [6], compared to 0.699 in Sugihara-Seki et al. [33] for neutral cylinders ($q_\mathrm{c} = 0$), and is approximately 0.95 (obtained from Fig. 8 of their paper) in the study of Bhalla and Deen [6], compared to 0.849 in the study of Sugihara-Seki et al. [33] for $q_\mathrm{c} = -0.01$ C/m^2 ($q_\mathrm{c}^* = -5.7$). Although the charge densities for albumin used in the analyses are not exactly the same, e.g., $q_\mathrm{s} = -0.02$ C/m^2 ($q_\mathrm{s}^* = -11.4$) in Bhalla and Deen [6], compared to $q_\mathrm{s} = -0.017$ C/m^2 ($q_\mathrm{s}^* = -9.5$) in Sugihara-Seki et al. [33], this cannot fully account for the differences in the osmotic reflection coefficient σ_v mentioned above. For reference, our obtained values of the filtration reflection coefficient σ_f for $a^* = 0.36$ and $q_\mathrm{s}^* = -11.4$ ($q_\mathrm{s} = -0.02$ C/m^2) are 0.780, 0.795, 0.897, 0.963 and 0.990 at $q_\mathrm{c}^* = 0, -0.51, -5.7, -15.2$ and -30.3, respectively, for $C_\infty = 0.15$ M ($\tau = 12.84$).

Zhang et al. [40] showed the equality of the filtration reflection coefficient σ_f and the osmotic reflection coefficient σ_v for the EGL model in the absence of charge effects, provided that the solute is convected at the local velocity of the suspending fluid. In the present study, however, we considered the lag of the solute behind the local fluid velocity due to the hydrodynamic interaction with surrounding cylinders. Accordingly, the filtration reflection coefficient σ_f is not necessarily equal to the osmotic reflection coefficient σ_v. In fact, a comparison of Fig. 9(b) for σ_f in the present study to Fig. 6 for σ_v in Sugihara-Seki et al. [33] indicates that σ_f is always larger than σ_v for the prescribed solute size, charge densities, and

ion concentration. This trend may be explained by the fact that the hydrodynamic interactions of the solute with surrounding cylinders hinder the transport of the solute as shown in Fig. 2(b).

Recently, Dechadilok and Deen [16] considered the hindered transport of charged spherical solute in a charged cylindrical pore. Although they studied the effect of the electrostatic double-layer distortion due to the solute motion, the electrostatic exclusion from pores, which decreases the partition coefficient, was found to be a far more important determinant of the overall diffusive permeability. Thus, we think it unlikely that the present results would change significantly when the retardation or polarization effect is included in the analysis.

At the entrance and exit of the EGL model, we have assumed that the solute concentrations just within the EGL are at equilibrium with the corresponding external concentrations $c_{u\infty}$ and $c_{d\infty}$, so that the Boltzmann distribution of solutes have been adopted under the condition that the solute potential vanishes outside of the EGL. This leads to Eqs (10) and (11), which provide the relationship between the averaged solute concentrations at both ends of the EGL model and the external concentrations in terms of the solute partition coefficient. Although this approach is consistent with Brenner and Gaydos [7] and Deen [17], hydrodynamic effects on the solute behavior near the entrance or exit have not been included. In addition, three-dimensional electric fields near both ends of the EGL model have not considered. There may be also a combined effect such that the solute trajectories are affected by the electric fields near the entrance and exit. As a problem of fluid dynamics, intensive studies have been made on the motion of a suspended particle near the entrance of a pore [12,13]. Quite recently, Oguro et al. [28] studied experimentally and theoretically the passage of a deformable particle through a pore, in relation to the transport of nanoparticles across the vessel wall including the EGL. They showed that the translation velocity of suspended particles is affected by the presence of the pore when the opening is approached within a few times of the pore diameter. Similarly, the entry length in the pore is estimated to be at most a few times of the pore diameter. Thus, we conclude that the hydrodynamic effect of the entrance or exit on the present results may not be significant since the spacing between adjacent cylinders is much smaller than the length of the cylinders. The electrostatic effect could be also insignificant in physiological states because of small values of the Debye length.

In the current study, we have focused on the case where the surface charges on the solute and cylinders are both negative ($q_s, q_c < 0$), since the EGL and serum albumin are known to carry negative charge. Evidently, the opposite case where both charges are positive can be treated in the same way, and the results of this work are directly applied to that case if q_s and q_c are changed from negative to positive sign. However, caution is necessary when the current model is applied to an attractive interaction between oppositely charged surfaces. In this case, solutes are more likely to approach the surface of cylinders due to the attractive force, so that the assumption of dilute solution employed here is invalidated near the cylinder surfaces. The treatment of this case is left for a future study.

The present model for the EGL was developed based on the experimental observation of a regular structure with a center-to-center fiber spacing of 20 nm and a fiber width of 12 nm for the EGL in the capillaries of the frog mesentery [31,38]. The EGL is a network of membrane-bound proteoglycans and glycoproteins, and both endothelium- and plasma-derived soluble molecules are integrated into this mesh [29,30,34,35,37]. Thus, the present model is an idealized model such that only the regular structure of core proteins is included. Recently, more detailed structural analyses showed evidence of similar structural regularity in the EGL of various mammalian microvessels [5]. Accordingly, although the present model is simple, it could provide insight into the transport properties of the EGL not just in frog mesentery capillaries, but also in various mammalian microvessels. A future study is expected to

provide a more detailed description of the transport of charged solutes through the EGL and to explore its control mechanism.

5. Conclusions

We have developed a fluid mechanical and electrostatic model for solute transport across an EGL model consisting of a layer of hexagonally ordered circular cylinders, and the partition coefficient, hindrance factors, and transport coefficients for the EGL are evaluated as functions of the charge densities, ion concentration and solute size. The present study suggests the important contribution of the electric charge to solute transport across the EGL and predicts a charge density in the EGL ranging from approximately -10 to -30 mEq/l in order to account for the experimental measurements of the reflection coefficient for serum albumin.

Acknowledgements

This research has been supported in part by a Grant-in-Aid for Scientific Research (B) (No. 23360087) from JSPS, the Special Research Fund of Kansai University and the Kansai University Grant-in-Aid for progress of research in graduate course.

References

[1] R.H. Adamson, V.H. Huxley and F.E. Curry, Single capillary permeability to proteins having similar size but different charge, *Am. J. Physiol*. **254** (1988), H304–H312.
[2] T. Akinaga, H. O-tani and M. Sugihara-Seki, Charge effects on hindrance factors for diffusion and convection of solute in pores II, *Fluid Dyn. Res*. **44** (2012), 065504.
[3] T. Akinaga, M. Sugihara-Seki and T. Itano, Electrical charge effect on osmotic flow through pores, *J. Phys. Soc. Jpn* **77** (2008), 053401.
[4] J.L. Anderson and D.M. Malone, Mechanism of osmotic flow in porous membranes, *Biophys. J*. **14** (1974), 957–982.
[5] K.P. Arkill, C. Knupp, C.C. Michell, C.R. Neal, K. Qvortrup, J. Rostgaard and J.M. Squire, Similar endothelial glycocalyx structures in microvessels from a range of mammalian tissues: Evidence for a common filtering mechanism?, *Biophys. J*. **101** (2011), 1046–1056.
[6] G. Bhalla and W.M. Deen, Effects of charge on osmotic reflection coefficients of macro-molecules in porous membranes, *J. Coll. Interface Sci*. **333** (2009), 363–372.
[7] H. Brenner and L.J. Gaydos, The constrained Brownian movement of spherical particles in cylindrical pores of comparable radius, *J. Coll. Interface Sci.* **58** (1977), 312–356.
[8] F.E. Curry, Mechanics and thermodynamics of transcapillary exchange, in: *Handbook of Physiology*, Vol. 4, E.M. Renkin and C.C. Michel eds, Am. Physiol. Soc., 1984, pp. 309–374.
[9] F.E. Curry and C.C. Michel, A fiber matrix model of capillary permeability, *Microvasc. Res*. **20** (1980), 96–99.
[10] F.E. Curry and T. Noll, Spotlight on microvascular permeability, *Cardiovasc. Res*. **87** (2010), 195–197.
[11] F.E. Curry, J.C. Rutledge and J.F. Lenz, Modulation of microvessel wall charge by plasma glycoprotein or osomucoid, *Am. J. Physiol. Heart Circ. Physiol*. **257** (1989), H1354–H1359.
[12] Z. Dagan, S. Weinbaum and R. Pfeffer, An infinite-series solution for the creeping motion through an orifice of finite length, *J. Fluid Mech*. **115** (1982), 505–523.
[13] Z. Dagan, S. Weinbaum and R. Pfeffer, Theory and experiment on the three-dimensional motion of a freely suspended spherical particle at the entrance to a pore at low Reynolds number, *Chem. Eng. Sci*. **38** (1983), 583–596.
[14] E.R. Damiano and T.M. Stace, A mechano-electrochemical model of radial deformation of the capillary glycocalyx, *Biophys. J*. **82** (2002), 1153–1175.
[15] P. Dechadilok and W.M. Deen, Hindrance factors for diffusion and convection in pores, *Ind. Eng. Chem. Res*. **45** (2006), 6953–6959.

[16] P. Dechadilok and W.M. Deen, Electrostatic and electrokinetic effects on hindered diffusion in pores, *J. Membrane Sci*. **336** (2009), 7–16.
[17] W.M. Deen, Hindered transport of large molecules in liquid-filled pores, *AIChE J*. **33** (1987), 1409–1425.
[18] B.M. Fu, B. Chen and W. Chen, An electrodiffusion model for effects of surface glycocalyx layer on microvessel permeability, *Am. J. Physiol. Heart Circ. Physiol.* **284** (2003), H1240–H1250.
[19] O. Kedem and A. Katchalsky, Thermodynamic analysis of the permeability of biological membranes to non-electrolytes, *Biochim. Biophys. Acta* **27** (1958), 229–246.
[20] O. Kedem and A. Katchalsky, A physical interpretation of the phenomenological coefficients of membrane permeability, *J. Gen. Physiol*. **45** (1961), 143–179.
[21] S. Kendall and C.C. Michel, The measurement of permeability in single rat venules using the red cell microperfusion technique, *Exp. Physiol*. **80** (1995), 359–372.
[22] D.G. Levitt, General continuum analysis of transport through pores. Part 1. Proof of Onsager's reciprocity postulate for uniform pore, *Biophys. J*. **15** (1975), 533–551.
[23] G. Li, W. Yuan and B.M. Fu, A model for the blood-brain barrier permeability to water and small solutes, *J. Biomech*. **43** (2010), 2133–2140.
[24] C.C. Michel, Starling: the formulation of his hypothesis of microvascular fluid exchange and its significance after 100 years, *Exp. Physiol*. **82** (1997), 1–30.
[25] C.C. Michel and F.E. Curry, Microvascular permeability, *Physiol. Rev*. **79** (1999), 703–761.
[26] M.I. Noble and A.J. Drake-Holland, Hyperglycaemia and the vascular glycocalyx: the key to microalbuminuria and cardiovascular disease in diabetes mellitus?, *Br. J. Diabetes Vasc. Dis.* **10** (2010), 66–70.
[27] H. O-tani, T. Akinaga and M. Sugihara-Seki, Charge effects on hindrance factors for diffusion and convection of solute in pores I, *Fluid Dyn. Res*. **43** (2011), 065505.
[28] Y. Oguro, M. Makino and O. Sano, Passage of a small air bubble through a circular pore across the plate of finite thickness, *J. Phys. Soc. Jpn* **79** (2010), 084402.
[29] A.R. Pries, T.W. Secomb and P. Gaehtgens, The endothelial surface layer, *Pflügers Archiv: Eur. J. Physiol.* **440** (2000), 653–666.
[30] S. Reitsma, D.W. Slaaf, H. Vink, M.A.M.J. van Zandvoort and M.G.A. oude Egbrink, The endothelial glycocalyx: composition, functions, and visualization, *Pflügers Archiv: Eur. J. Physiol*. **454** (2007), 345–359.
[31] M. Squire, M. Chew, G. Nneji, C. Neal, J. Barry and C.C. Michel, Quasi-periodic substructure in the microvessel endothelial glycocalyx: a possible explanation for molecular filtering?, *J. Struct. Biol*. **136** (2001), 239–255.
[32] M. Sugihara-Seki, Transport of spheres suspended in the fluid flowing between hexagonally arranged cylinders, *J. Fluid Mech*. **551** (2006), 309–321.
[33] M. Sugihara-Seki, T. Akinaga and T. Itano, Effects of electric charge on osmotic flow across periodically arranged circular cylinders, *J. Fluid Mech.* **664** (2010), 174–192.
[34] J.M. Tarbell, Shear stress and the endothelial transport barrier, *Cardiovasc. Res*. **87** (2010), 320–330.
[35] J.M. Tarbell and M.Y. Pahakis, Mechanotransduction and the glycocalyx, *J. Intern. Med.* **259** (2006), 339–350.
[36] S. Weinbaum, 1997 Whitaker distinguished lecture: model to solve mysteries in biomechanics at the cellular level; a new view of fiber matrix layers, *Ann. Biomed. Eng.* **26** (1998), 627–643.
[37] S. Weinbaum, J.M. Tarbell and E.R. Damiano, The structure and function of the endothelial glycocalyx layer, *Ann. Rev. Biomed. Eng*. **9** (2007), 121–167.
[38] S. Weinbaum, X. Zhang, Y. Han, H. Vink and S.C. Cowin, Mechanotransduction and flow across the endothelial glycocalyx, *PNAS* **100** (2003), 7988–7995.
[39] W. Yuan, G. Li and B.M. Fu, Modulation of the blood-brain barrier permeability by plasma glycoprotein orosomucoid, *Microvasc. Res*. **80** (2010), 148–157.
[40] X. Zhang, F. Curry and S. Weinbaum, Mechanism of osmotic flow in a periodic fiber array, *Am. J. Physiol. Heart Circ. Physiol*. **290** (2006), H844–H852.